aVsIs: An Analytical-Solution-Based Solver for Model-Predictive Control With Hexagonal Constraints in Voltage-Source Inverter Applications

Ismaele Diego De Martin, Dario Pasqualotto, *Member, IEEE*, and Fabio Tinazzi, *Member, IEEE*

***Abstract*—The theory of a new analytical-solution-based algorithm for calculating the optimal solution in model-predictive control applications with hexagonal constraints is discussed in this article. Three-phase voltage-source inverters for power electronic and electric motor drive applications are the target of the proposed method. The indirect model-predictive control requires a constrained quadratic programming (QP) solver to calculate the optimal solution. Most of the QP solvers use numerical algorithms, which may result in unbearable computational burdens. However, the optimal constrained solution can be calculated in an analytical way when the control horizon is limited to the first step. A computationally efficient algorithm with a certain maximum number of operations is proposed in this article. A thorough mathematical description of the solver in both the stationary and rotating reference frames is provided. Experimental results on real test rigs featuring either an electric motor or a resistive–inductive load are reported to demonstrate the feasibility of the proposed solver, thus smoothing the way for its implementation in industrial applications. The name of the proposed solver is `aVsIs`, which is released under Apache License 2.0 in GitHub, and a free example is available in Code Ocean.**

***Index Terms*—Continuous control set (CCS), interior permanent magnet (IPM), model-predictive control (MPC), permanent magnet synchronous motor (PMSM), synchronous reluctance (SynR).**

I. Introduction

THE model-predictive control (MPC) paradigm is popular in the scientific research community working in the power electronic and electric drive application fields. Two different MPC technique groups can be found, namely, *direct* and *indirect* MPC algorithms [1]–[3]. The former techniques do not require a voltage modulator, e.g., the space vector modulation, whereas the latter techniques do.

The direct MPC techniques gained the spotlight due to their simplicity of application and relative modest computational effort. In a nutshell, the control algorithm considers the direct application of the available voltage vectors to the plant, e.g., an electric motor. These algorithms are also known as *finite-set* MPC [4], since the number of voltage vectors that can be applied is limited to the base voltage vectors. However, the direct MPC techniques are unsuitable in those applications, where the switching frequency should be precisely known and the current ripple kept as low in magnitude as possible [5].

The indirect MPC techniques can provide a smooth current tracking behavior and constant switching frequency, although the computational burden required by the solver can be a cumbersome aspect. Conversely to the finite-set MPC algorithms, the available voltage set among which selecting the optimal solution is *continuous*, the indirect algorithms are also known as *continuous-set* MPC [6]. The continuous-set MPC strategies require a modulator for generating the voltage reference, which returns several advantages in terms of harmonic distortions and current ripple at the price of a more complex implementation [7]. The optimal solution is calculated by solving a constrained problem due to the presence of voltage limitations.

The control structure of the power electronic and electric motor drive applications allows us to define quadratic programming (QP) problems for current control tracking. So far, several QP solvers have been proposed for the real-time implementation of continuous-set MPC algorithms [8]. However, these solvers were designed for general (or all purpose) QP problems, and they have not been optimized for particular cases. The `acados` project in [9] reports a vast list of QP solvers for embedded optimization. A more general approach was preferred for `acados`, i.e., the solvers were not designed for specific problems, at the price of more computational burden. In turn, general solvers cannot provide an analytical solution since numerical-based algorithms [9], [10] are implemented. With regard to power electronic applications, all the general QP solvers do not take advantage from the knowledge of the constraint formulation of the voltage-source inverter. In general, the computational effort required by the QP solver has always been a source of concern in the application of indirect MPC algorithms [11]–[14], and it

Manuscript received 7 October 2021; revised 17 February 2022, 31 March 2022, and 8 June 2022; accepted 19 July 2022. Date of publication 26 July 2022; date of current version 6 September 2022. This work was supported by the Department of Management and Engineering, University of Padova, through the Research Project "Interdisciplinary Strategy for the Development of Advanced Mechatronics Technologies" under Grant CUP-C36C18000400001. Recommended for publication by Associate Editor H. L. Ginn. *(Corresponding author: Fabio Tinazzi.)*

The authors are with the Department of Management and Engineering, University of Padova, 36100 Vicenza, Italy (e-mail: ismaelediego.demartin@phd.unipd.it; dario.pasqualotto@unipd.it; fabio.tinazzi@unipd.it).

Color versions of one or more figures in this article are available at https://doi.org/10.1109/TPEL.2022.3193807.

Digital Object Identifier 10.1109/TPEL.2022.3193807

has hindered the continuous-control-set (CCS) MPC implementation on industrial applications.

The implicit methods are gaining considerable attention in the power electronic and electric drive fields. It has been applied for LC filters in [15] and [16]. The current control of the electric motor drive is often subject to the advanced MPC algorithm, such as integral MPC in [11], nonlinear MPC in [12], and data-driven-based MPC in [17]. A speed control of isotropic synchronous motors has been considered in [18], where particular attention has been paid to reduce the computational burden. Therefore, the call for a more efficient QP solver dedicated to power electronic application is strong, since it can smooth the implementation of the advanced MPC algorithm. Furthermore, the indirect methods are of particular interest in special applications, such as the multiphase motors, i.e., a motor with more than three phases. In these special motors, the field-oriented control is very important (see [19]–[21]), and effective MPC current control algorithms can benefit from a computationally efficient solver. The work proposed in [22] requires a modification of the cost function by adding an additional parameter, thus leading to suboptimal solutions. The work in [23] considers modular multilevel converters, and the solution of the optimization problem is obtained from a geometrical interpretation. However, the fast QP solver tailored for hexagonal constrained solutions for voltage-source inverters is still an open issue.

An analytical-solution-based solver suitable for QP problems in CCS-MPC algorithms adopted in the voltage-source inverter with hexagonal constraints is discussed in this article. The proposed solver name is `aVsIs`. The hexagonal constraints introduced by the inverter are taken into account, and the worst-case situation, i.e., the maximum number of required calculations, is discussed. The solver `aVsIs` is a complete novelty in the continuous-set MPC solver panorama, since it involves neither numerical algorithms nor cost function formulation modifications. The algorithm implementation is demonstrated for the current control task in electric motor drive and resistive–inductive load applications. The current control problem is formulated either in the stationary $\alpha\beta$ and rotating dq reference frames for the sake of generality.

The rest of this article is organized as follows. The theory of a CCS-MPC algorithm for power electronic and electric motor drive applications is described in Section II. The detailed explanation of the proposed analytical-solution-based solver for problems formulated in the stationary $\alpha\beta$ reference frame is discussed in Section III, whereas the solver application to problems formulated in the rotating dq reference frame is explained in Section IV. The effectiveness of `aVsIs` was tested by means of simulation and experimental tests that are reported and commented in Section V. Finally, Section VI concludes this article.

II. Theory of Operations for MPC Algorithms

The quadratic cost function of an indirect continuous-set MPC problem is

$$J = \sum_{j=0}^{N-1} \|\mathbf{x}^*(k+j+1) - \mathbf{x}(k+j+1)\|_{\mathbf{Q}}^2$$

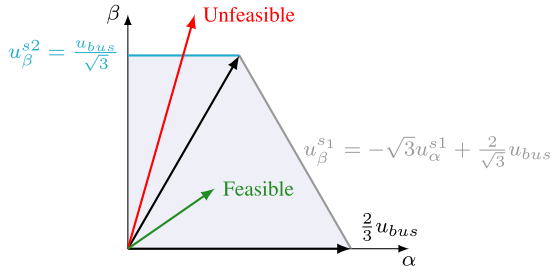

Fig. 1. Voltage constraints in the first quadrant.

$$+ \sum_{i=0}^{N_u-1} \|\mathbf{u}(k+i+1) - \mathbf{u}(k+i)\|_{\mathbf{R}}^2 \tag{1}$$

where N and N_u are the prediction and the control horizon, respectively, $\mathbf{Q}$ is the state tracking weights matrix,[1] $\mathbf{R}$ is the control effort penalization matrix, $\mathbf{x}$ and $\mathbf{x}^*$ are the state and reference state vectors, respectively, and $\mathbf{u}$ is the vector of control variables. In general, the optimization problem that has to be solved at each control time k is

$$\begin{aligned} \min_{\mathbf{u}} \quad & J \\ \text{s.t.} \quad & \mathbf{x}(k+1) = \mathbf{F}\mathbf{x}(k) + \mathbf{G}\mathbf{u}(k) \\ & \mathbf{u} = [\mathbf{u}(k+1), \ldots, \mathbf{u}(k+N_u)] \in \mathbf{U} \end{aligned} \tag{2}$$

where $\mathbf{F}$ and $\mathbf{G}$ are generic state-space matrices and $\mathbf{U} \in \mathbb{R}^{2N_u}$ represents the feasible solution set.

The feasible solution set considered in this article is $\mathbf{U} \in \mathbb{R}^2$, which means $N_u = 1$. Actually, the control horizon $N_u = 1$ is a necessary condition for the proposed solver to keep the computational burden at bay. In many applications, especially when the control frequency is high, the control horizon can be much smaller than the prediction horizon. The feasible set $\mathbf{U}$ in the fixed reference frame depicts a hexagon region in the $\alpha\beta$ plane, as sketched in the example of Fig. 1.

In order to obtain a feasible solution, the following inequalities must be satisfied:

$$\begin{aligned} & \mathbf{A}\mathbf{u}(k+1) \le \mathbf{b} \\ & \mathbf{A} = \begin{bmatrix} \sqrt{3} & 0 & -\sqrt{3} & -\sqrt{3} & 0 & \sqrt{3} \\ 1 & 1 & 1 & 1 & 1 & 1 \end{bmatrix}^T \\ & \mathbf{b} = \frac{u_{\text{bus}}}{\sqrt{3}} \begin{bmatrix} 2 & 1 & 2 & 2 & 1 & 2 \end{bmatrix}^T \end{aligned} \tag{3}$$

where u_{bus} is the bus voltage. The condensed problem (2) is rewritten as a quadratic problem as follows:

$$\begin{aligned} & \min_{\mathbf{u}(k+1)} J(\mathbf{u}(k+1)) \triangleq \frac{1}{2}\mathbf{u}(k+1)^T\mathbf{H}\mathbf{u}(k+1) + \mathbf{f}^T\mathbf{u}(k+1) \\ & s.t. \quad \mathbf{A}\mathbf{u}(k+1) \le \mathbf{b} \end{aligned} \tag{4}$$

[1] One should recall that $\|\boldsymbol{\xi}\|_{\boldsymbol{\Phi}}^2 = \boldsymbol{\xi}^T\boldsymbol{\Phi}\boldsymbol{\xi}$, where $\boldsymbol{\Phi}$ is a weighting matrix.

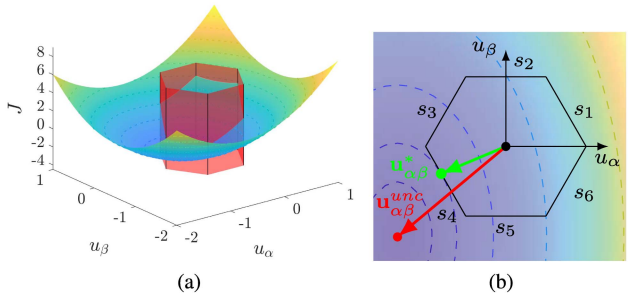

Fig. 2. (a) Example of the quadratic cost function surface and (b) its top view. Dashed lines represent the constant value loci of the cost function.

where

$$\mathbf{H} \triangleq \begin{bmatrix} h_1 & h_2 \\ h_3 & h_4 \end{bmatrix}; \qquad \mathbf{f} \triangleq \begin{bmatrix} f_1 \\ f_2 \end{bmatrix}. \tag{5}$$

The matrix $\mathbf{H}$ and the vector $\mathbf{f}$ vary with the problem at hand. Different MPC algorithms, either implementing disturbance observer, data-driven, or model-free control paradigms for offset-free current tracking, can be described by (4).

A. Hypothesis of the aVsIs Algorithm

Matrix $\mathbf{H}$ is assumed to be symmetric and positive definite (i.e., all the eigenvalues are positive and not null), which is the case for most of the power electronic and electric drive applications [12], [24]. Thus, the problem (4) is strictly convex, and the cost function can be graphically represented by an elliptic paraboloid with only one minimum [25]. The unconstrained solution can always be calculated in closed form as

$$\mathbf{u}^{\text{unc}}(k+1) = -\mathbf{H}^{-1}\mathbf{f}. \tag{6}$$

This solution can be directly applied to the inverter, provided that inequality (3) is satisfied. In other words, (6) is already the optimal solution if the correspondent voltage vector $\mathbf{u}^{\text{unc}}(k+1)$ lies inside the hexagonal boundaries (see Fig. 1). When the voltage vector obtained by (6) is unfeasible (see Fig. 1), the actual optimal solution lies on the boundary of the feasible voltage set $\mathbf{U}$, i.e., on one side of the hexagon.

An important choice for the proposed method is the control horizon value, which is set as $N_u = 1$, whereas the prediction horizon N can be of arbitrary value. The single-step control horizon means that $\mathbf{u}(k+1) \in \mathbb{R}^{2\times 1}$. It is worth highlighting that $N_u = 1$ is a very common choice in all the applications with reduced computational power. The general QP solvers (see [9]) require a high computational burden, which further increases when a longer prediction horizon, i.e., $N_u > 1$, is considered.

A 3-D representation of the cost function with minimum outside the feasible region is shown in Fig. 2(a). In the example, the solution of (6) is unfeasible. The feasible region is highlighted by a hexagonal shape polyhedron. The same cost function is sketched in the 2-D representation of Fig. 2(b). The feasible optimal solution lies on one of the sides of the hexagon. It is important to highlight that the feasible optimal solution does not always correspond to applying the voltage saturation on the global optimal solution by means of the voltage modulator. The minimum cost function value can be obtained in correspondence to the curve tangent to the hexagon of Fig. 2(b). This condition is often verified in those power electronic applications where part of the plant under control is affected by magnetic saturation, such as in anisotropic electric motors.

In a nutshell, the solver aVsIs requires a problem formulated such that the output is $\mathbf{u}(k+1) \in \mathbb{R}^{2\times 1}$, $\mathbf{H}$ being positive definite, and it does not require restrictions about the state variables. For instance, $\mathbf{x}$ can be either currents or magnetic fluxes.

B. Problem Formulation for an RL Circuit

The discrete dynamic equations in the stationary reference frame $\alpha\beta$ of an RL circuit are

$$\mathbf{i}_{\alpha\beta}(k+1) = \mathbf{F}\mathbf{i}_{\alpha\beta}(k) + \mathbf{G}\mathbf{u}_{\alpha\beta}(k) \tag{7}$$

where $\mathbf{i}_{\alpha\beta} = [i_\alpha\, i_\beta]^T$ and $\mathbf{u}_{\alpha\beta} = [u_\alpha\, u_\beta]^T$ are the $\alpha\beta$ currents and voltages, respectively. Furthermore, the following matrices are defined:

$$F = \begin{bmatrix} 1 - \dfrac{RT_c}{L} & 0 \\ 0 & 1 - \dfrac{RT_c}{L} \end{bmatrix}, \quad G = \begin{bmatrix} \dfrac{T_c}{L} & 0 \\ 0 & \dfrac{T_c}{L} \end{bmatrix} \tag{8}$$

where R and L are the resistance and inductance values, respectively, and T_c is the control period. Considering $N = N_u = 1$, $\mathbf{Q} = \mathbf{I} \in \mathbb{R}^2$, and $\mathbf{R} = \text{diag}(\eta_\alpha, \eta_\beta)$, the matrix values of $\mathbf{H}$ and $\mathbf{f}$ in (4) can be written as

$$\begin{aligned} h_1 &= 2\left[\left(\frac{T_c}{L}\right)^2 + \eta_\alpha\right]; \quad h_4 = 2\left[\left(\frac{T_c}{L}\right)^2 + \eta_\beta\right] \\ h_2 &= h_3 = 0 \\ f_1 &= -2\left[\left(i^*_\alpha - i_\alpha(k+1)\frac{RT_c}{L}\right)\frac{T_c}{L} + \eta_\alpha u_\alpha\right] \\ f_2 &= -2\left[\left(i^*_\beta - i_\beta(k+1)\frac{RT_c}{L}\right)\frac{T_c}{L} + \eta_\beta u_\beta\right]. \end{aligned} \tag{9}$$

It is worth highlighting that the problem formulation for the current control of an electric motor drive is very similar to an RL circuit one. Equations (7) and (8) resemble the model of electric motors, which can be obtained by including the magnetic fluxes and speed-dependent terms, such as in [12].

III. aVsIs Algorithm in the $\alpha\beta$ Reference Frame

In the case of unfeasible voltage vector from (6), the solution must be found on one of the sides of the hexagon. Each side of the hexagon is considered the segment of a family of straight lines, whose equations are reported in Table I. The hexagonal side equations are substituted into the cost function (4); thus, the problem formulation depends on one variable, and a closed-form analytical solution can be found.

To ease the discussion, only one hexagon side straight line equation is considered in the following, but the same procedure is carried out on each side using the equations in Table I. The cost function adopted in (4) is rewritten in its extended form (the

TABLE I
HEXAGON STRAIGHT LINE EQUATIONS

Side	Straight line equation	Domain
s_1	$u_\beta = -\sqrt{3}u_\alpha + \frac{2u_{\text{bus}}}{\sqrt{3}}$	$u_\alpha \in \left(\frac{u_{\text{bus}}}{3}, \frac{2u_{\text{bus}}}{3}\right)$
s_2	$u_\beta = \frac{u_{\text{bus}}}{\sqrt{3}}$	$u_\alpha \in \left(-\frac{u_{\text{bus}}}{3}, \frac{u_{\text{bus}}}{3}\right)$
s_3	$u_\beta = \sqrt{3}u_\alpha + \frac{2u_{\text{bus}}}{\sqrt{3}}$	$u_\alpha \in \left(-\frac{2u_{\text{bus}}}{3}, -\frac{u_{\text{bus}}}{3}\right)$
s_4	$u_\beta = -\sqrt{3}u_\alpha - \frac{2u_{\text{bus}}}{\sqrt{3}}$	$u_\alpha \in \left(-\frac{2u_{\text{bus}}}{3}, -\frac{u_{\text{bus}}}{3}\right)$
s_5	$u_\beta = -\frac{u_{\text{bus}}}{\sqrt{3}}$	$u_\alpha \in \left(-\frac{u_{\text{bus}}}{3}, \frac{u_{\text{bus}}}{3}\right)$
s_6	$u_\beta = \sqrt{3}u_\alpha - \frac{2u_{\text{bus}}}{\sqrt{3}}$	$u_\alpha \in \left(\frac{u_{\text{bus}}}{3}, \frac{2u_{\text{bus}}}{3}\right)$

time dependence k is dropped)

$$J(u_\alpha, u_\beta) = \frac{1}{2}\left(u_\alpha^2 h_1 + u_\beta^2 h_4 + (h_2 + h_3)u_\alpha u_\beta\right) + u_\alpha f_1 + u_\beta f_2. \tag{10}$$

The equation of the first hexagon side constraints, i.e., the segment between the first and second active vectors in the voltage plane, can be written as

$$u_\beta = \frac{2u_{\text{bus}}}{\sqrt{3}} - \sqrt{3}u_\alpha. \tag{11}$$

The first side corresponds to s_1 in Fig. 2(b), where the names of the remaining five sides are also defined. By substituting (11) into (10), the unknown term of the cost function J reduces to u_α, i.e.,

$$J(u_\alpha) = \frac{1}{2}\left[u_\alpha^2 h_1 + \left(\frac{2u_{\text{bus}}}{\sqrt{3}} - \sqrt{3}u_\alpha\right)^2 h_4\right] + \frac{1}{2}\left[(h_2 + h_3)u_\alpha\left(\frac{2u_{\text{bus}}}{\sqrt{3}} - \sqrt{3}u_\alpha\right)\right] + u_\alpha f_1 + \left(\frac{2u_{\text{bus}}}{\sqrt{3}} - \sqrt{3}u_\alpha\right) f_2. \tag{12}$$

In order to find the minimum of (12), thus one possible optimal solution, one has to calculate the value $u_\alpha^{s_1}$ that satisfies

$$\left.\frac{dJ(u_\alpha)}{du_\alpha}\right|_{u_\alpha = u_\alpha^{s1}} = 0. \tag{13}$$

The possible $u_\beta^{s_1}$ optimal solution value is calculated by substituting the solution of (13) into (11). The complete set of calculations for hexagon side s_1 is

$$u_\alpha^{s_1} = -\frac{f_1 - 2u_{\text{bus}}h_4 - \sqrt{3}f_2 + \frac{u_{\text{bus}}(h_2 + h_3)}{\sqrt{3}}}{h_1 + 3h_4 - \sqrt{3}(h_2 + h_3)}$$
$$u_\beta^{s_1} = \frac{2u_{\text{bus}}}{\sqrt{3}} - \sqrt{3}u_\alpha^{s_1}. \tag{14}$$

Similar sets of equations are obtained for each side of the hexagon, which are not reported in this article due to space length limitations. However, the procedure is to substitute each of the straight line equations reported in Table I into (13), where J is formulated as in (10), and then calculate the resulting voltage u_α. The calculation of u_β is trivial.

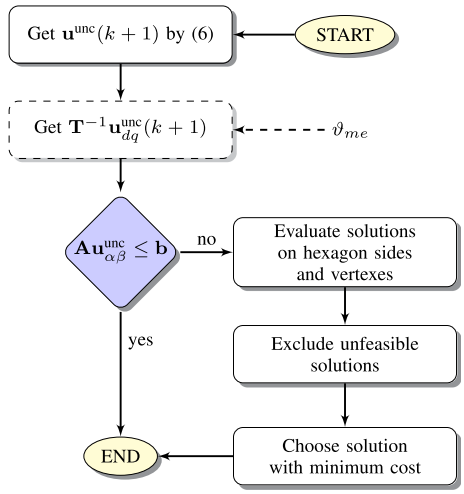

Fig. 3. Flowchart of the aVsIs algorithm. The dashed block is carried out when using the *dq* formulation.

The solution $\mathbf{u}_{\alpha\beta}(k+1)$ calculated with (14) is feasible if the voltage $u_\alpha^{s_1}$ lies in the domain reported in Table I. In the example of (14), the domain of the first constraint is $u_\alpha \in (u_{\text{bus}}/3\,,\, 2u_{\text{bus}}/3)$. All six solutions must be verified within the domains reported in Table I. The solutions corresponding to the six hexagon vertices have to be also considered. In particular working conditions, such as at high speed in electric drives or during fast current transients, the optimal solution may lie in one of the hexagonal vertices. This case occurs when all the six solutions calculated on the hexagon sides lie outside the domains of Table I. Finally, the solution that returns the minimum cost of (10) is chosen as the optimal one.

A. Algorithm Steps

A step-by-step description of the proposed solver is provided in this section for the sake of clarity. The entire procedure is sketched in the flowchart of Fig. 3. The detailed description of the proposed solver is as follows.

1) Get an unconstrained solution $\mathbf{u}_{\alpha\beta}^{\text{unc}}(k+1)$ by means of (6).
2) If the unconstrained solution $\mathbf{u}_{\alpha\beta}^{\text{unc}}(k+1)$ does not satisfy (3), six solutions are calculated on each side of the hexagon and six solutions for all the hexagon vertices.
3) The feasibility of each solution on the hexagon sides is verified by checking that they belong to the respective domain of Table I.
4) The cost of feasible solutions is calculated, and the optimal solution corresponds to the one with the lowest cost.

Due to the monotonic behavior of (4) in $\mathbb{R}^2$, an optimal solution within the hexagon region (see example in Fig. 2) is always present.

IV. aVsIs ALGORITHM IN THE *dq* REFERENCE FRAME

The MPC problem is formulated in the dq reference frame in many application cases, such as the electric motor drives [26], [27]. The proposed solver can be adapted accordingly.

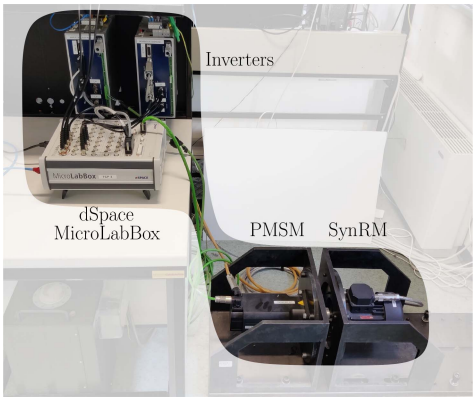

Fig. 4. Test rig for $\alpha\beta$ in Section III or dq solver in Section IV. The position ϑ_{me} is necessary for dq problems.

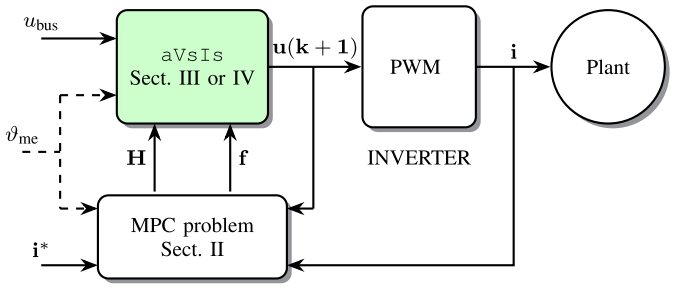

Fig. 5. Experimental setup.

The extended form of the cost function adopted in (15) and expressed in dq is

$$J(u_d, u_q) = \frac{1}{2}\left(u_d^2 h_1 + u_q^2 h_4 + (h_2 + h_3) u_d u_q\right) + u_d f_1 + u_q f_2. \tag{15}$$

The inequality constraint (3) is modified as follows:

$$\mathbf{A}\mathbf{T}^{-1}(\vartheta_{\text{me}})\mathbf{u}_{dq}(k+1) \leq \mathbf{b} \tag{16}$$

where $\mathbf{T}(\vartheta_{\text{me}})$ is the Park transformation, whereas $\mathbf{A}$ and $\mathbf{b}$ are the ones defined in (3). ϑ_{me} can be the electric position in electric motor drive applications or the grid phase in power electronic applications. Therefore, the proposed solver discussed in Section III can be applied by considering that $\mathbf{u}_{\alpha\beta} = \mathbf{T}^{-1}(\vartheta_{\text{me}})\mathbf{u}_{dq}$.

For the sake of simplicity, only one side of the hexagon is considered, as it has been done for the $\alpha\beta$ solver in Section III. It is worth recalling that the same mathematical steps are applied to the remaining five hexagon sides by using the straight line equations in Table I. The first constraint equation (11) can be rewritten as

$$(S + \sqrt{3}C)u_d + (C - \sqrt{3}S)u_q = \frac{2u_{\text{bus}}}{\sqrt{3}} \tag{17}$$

where $S \triangleq \sin(\vartheta_{\text{me}})$ and $C \triangleq \cos(\vartheta_{\text{me}})$ have been defined to ease the mathematical notation. A one-variable cost function can be written by rearranging (17) and highlighting either u_d or u_q and then substituting its expression into (15). Both u_d and u_q can be chosen for the substitution in the cost function. The choice that returns a feasible solution has to be selected.

The computation of the solutions along the hexagon sides can be troublesome due to the reference frame transformation in (16). Let u_d be the selected variable, i.e., the problem to solve is

$$\frac{dJ(u_d)}{du_d} = 0. \tag{18}$$

After some tedious calculations, the analytical solution of (18) along the first side of the hexagon is obtained as

$$u_d^{s_1} = -\frac{f_1 - \eta_1 f_2 + \eta_2(h_2 + h_3) - \eta_3 h_4}{h_1 - \eta_1(h_2 + h_3) + \eta_4 h_4} \tag{19}$$

where the coefficients η_i, $i = 1, \ldots, 4$, are calculated as

$$\eta_1 = \frac{S + \sqrt{3}C}{C - \sqrt{3}S} \qquad \eta_2 = \frac{u_{\text{bus}}}{\sqrt{3}} \frac{1}{C - \sqrt{3}S}$$
$$\eta_3 = \frac{2u_{\text{bus}}}{\sqrt{3}} \frac{S + \sqrt{3}C}{(C - \sqrt{3}S)^2} \quad \eta_4 = \left(\frac{S + \sqrt{3}C}{C - \sqrt{3}S}\right)^2. \tag{20}$$

The q-axis voltage reference solution is

$$u_q^{s_1} = \frac{2u_{\text{bus}}}{\sqrt{3}} - \eta_1 u_d^{s_1}. \tag{21}$$

Equations (19) and (21) can be calculated by a microprocessor only if the coefficients in (20) are real and finite numbers. Therefore, $C - \sqrt{3}S \neq 0$ should be always verified. However, it holds that $C - \sqrt{3}S = 0$ for $\vartheta_{\text{me}} = \pi/6 + n\pi$, $n \in \mathbb{Z}$, and the solution to (18) cannot be calculated. In order to sort out this shortcoming, the analytical solution is computed by using u_q instead of u_d as minimization variable in (18), obtaining

$$u_q^{s_1} = -\frac{f_2 - \eta_1 f_1 + \eta_2(h_2 + h_3) - \eta_3 h_4}{h_4 - \eta_1(h_2 + h_3) + \eta_4 h_1}$$
$$u_d^{s_1} = \frac{2u_{\text{bus}}}{\sqrt{3}} - \eta_1 u_d^{s_1} \tag{22}$$

where the coefficient η_i, $i = 1, \ldots, 4$, are recalculated as

$$\eta_1 = \frac{C - \sqrt{3}S}{S + \sqrt{3}C}, \qquad \eta_2 = \frac{u_{\text{bus}}}{\sqrt{3}} \frac{1}{S + \sqrt{3}C}$$
$$\eta_3 = \frac{2u_{\text{bus}}}{\sqrt{3}} \frac{C - \sqrt{3}S}{(S + \sqrt{3}C)^2}, \qquad \eta_4 = \left(\frac{C - \sqrt{3}S}{S + \sqrt{3}C}\right)^2. \tag{23}$$

Considering the denominator of each η_i in (20) and (23), it follows that they are not zero at the same time since $C - \sqrt{3}S = 0$ for $\vartheta_{\text{me}} = \pi/6 + n\pi$, $n \in \mathbb{Z}$ and $S + \sqrt{3}C = 0$ for $\vartheta_{\text{me}} = \pi/3 + n\pi$, $n \in \mathbb{Z}$.

Similar considerations can be made for all the other constraints related to the remaining five sides of the hexagon. The formulation of the sets of solutions does not change, provided that the hypothesis of Section II-A is verified. Therefore, the sets of solutions can be translated into programming code. The algorithm steps of the proposed solver in $\alpha\beta$ discussed in Section III-A and sketched in Fig. 3 are modified as follows.

1) If the unconstrained solution $\mathbf{u}_{dq}^{\text{unc}}$ does not satisfy (16), the optimal solution lies on the hexagon sides.

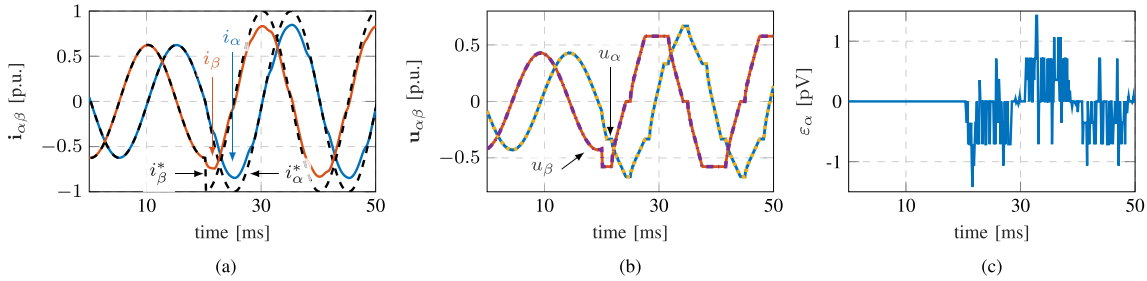

Fig. 6. Simulation results with aVsIs ($\alpha\beta$ version). A reference current step variation was forced at 20 ms. (a) $\alpha\beta$ current response using aVsIs. (b) aVsIs (solid lines), qpOASES (dotted). (c) aVsIs and qpOASES solution difference.

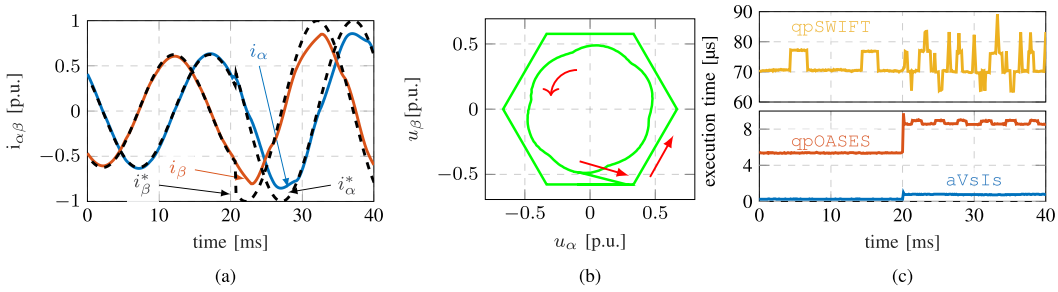

Fig. 7. Experimental results with aVsIs ($\alpha\beta$ version). A reference current step variation was forced at 20 ms. (a) $\alpha\beta$ current response. (b) $\alpha\beta$ voltage trajectory. (c) Execution time.

TABLE II
NUMBER OF ALGEBRAIC OPERATIONS OF aVsIs

Parameter	$\alpha\beta$ solver	dq solver
Sum/sub	86	125
Product	174	229
Division	4	10

2) In order to calculate the solutions on the hexagon sides and vertices, the cost function is calculated for either d-axis, such as in (19) and (21), or q-axis, such as in (22). The choice has to be made based on the presence of impossible solutions, i.e., by verifying that the denominator of the coefficients η_i is not zero.
3) The feasibility of each solution is checked in the $\alpha\beta$ reference frame (see domains in Table I).
4) The cost of feasible solutions is calculated, and the optimal solution corresponds to the one with the lowest cost.

V. RESULTS AND DISCUSSION

In order to evaluate the applicability of aVsIs on a specific microcontroller, a quantitative evaluation of the number of calculations was carried out. A number of operations, namely, algebraic sums, multiplications, and divisions, were considered, and the total amount is listed in Table II. It is worth pointing out that the proposed solver does not require the voltage saturation in the modulator, since the voltage to be synthesized is always feasible. Therefore, the pulsewidth modulation algorithm can be simplified compared to conventional applications. Since only basic mathematics operations and if-statement are employed, the proposed solver computations can be implemented in a field-programmable gate array, thus further reducing the computational time required to obtain the optimal solution.

The aVsIs solver was tested on different test rigs all featuring a dSPACE MicrolabBox for rapid control prototyping. The structure of the predictive current control algorithm is similar for power electronic and electric motor drive applications, and it has been sketched in Fig. 4. Two different applications are considered in this article, i.e., two different *plants* in Fig. 4. The first example is the current control in the $\alpha\beta$ reference frame of an RL circuit by adopting the algorithm proposed in Section II-B. The second example is the current control in the dq reference frame of a synchronous reluctance (SynR) motor drive. The results are reported in Section V-B. A reduced u_{bus} voltage was adopted for each case aiming at forcing the solver to find the optimal solution of the MPC problem alongside the hexagonal edges even at low speed or current, which is the worst-case scenario in terms of execution time. It is worth highlighting that the operations at full bus voltage are still guaranteed. The sampling and switching frequency were both set at 8 kHz for all the tests reported in this section. A photograph of the experimental test rig is reported in Fig. 5. All the measurements were normalized with respect to the nominal values reported in Tables III and IV. The voltages were normalized with respect to the bus voltage value.

Two general QP solvers were implemented for the sake of comparison. The first one is the MATLAB *quadprog* solver, which implements the qpOASES algorithm [10] when the *active set* option is selected. The qpOASES algorithm is an open-source and computationally efficient algorithm written in C language, specifically designed for generic real-time applications.

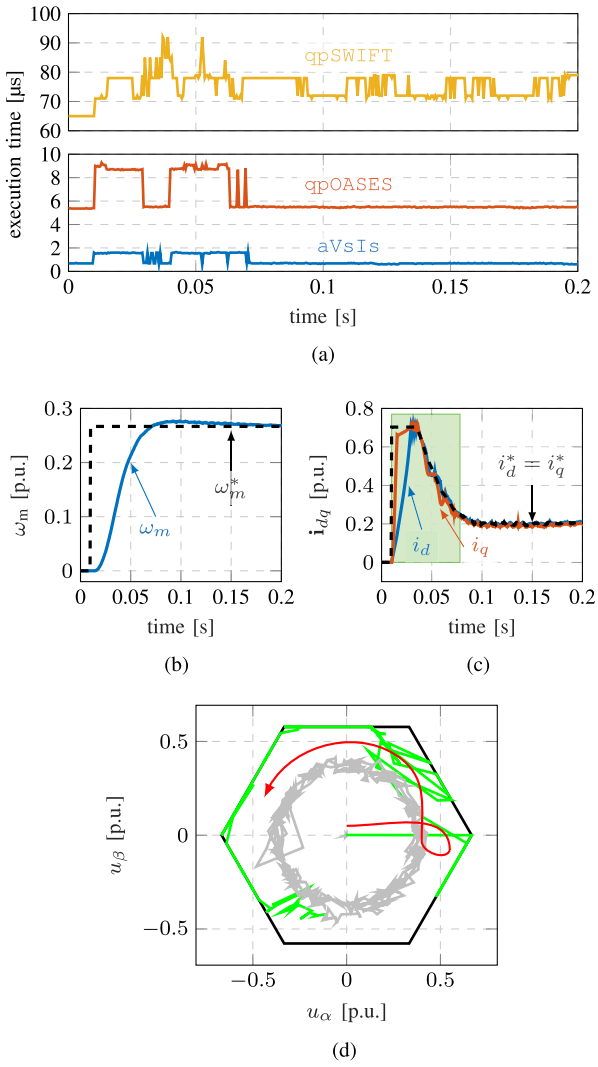

Fig. 8. Experimental results of the aVsIs (dq version) solver for a SynR motor. (a) Comparison in terms of execution time of different solvers. (b) Speed response. (c) Currents response. (d) $\alpha\beta$ voltage trajectory.

TABLE III
SYSTEM PARAMETERS FOR THE $\alpha\beta$ SOLVER TEST

Parameter	Symbol	Unit	Value
DC voltage	u_{bus}	V	60
Nominal frequency	f_N	Hz	50
Nominal current	I_N	A	8
Resistance	R	Ω	2.15
Inductance	L	mH	2

The second one is the qpSWIFT solver, which is a real-time sparse QP solver for embedded applications [28].

A. *Validation of the* aVsIs *Solver in* $\alpha\beta$

A simulation of the test rig featuring an RL plant, whose parameters are reported in Table III, was carried out aiming at demonstrating the optimal solution characteristic calculated by

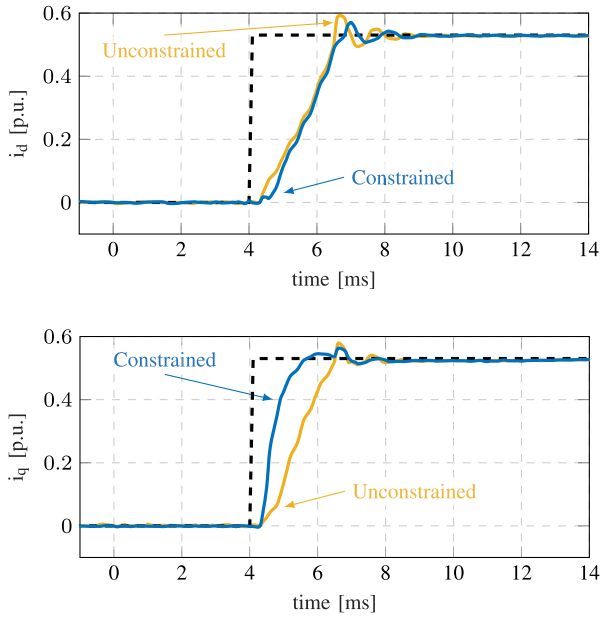

Fig. 9. Current dynamics using constrained or unconstrained solutions when the SynR motor is dragged at 25% ω_n.

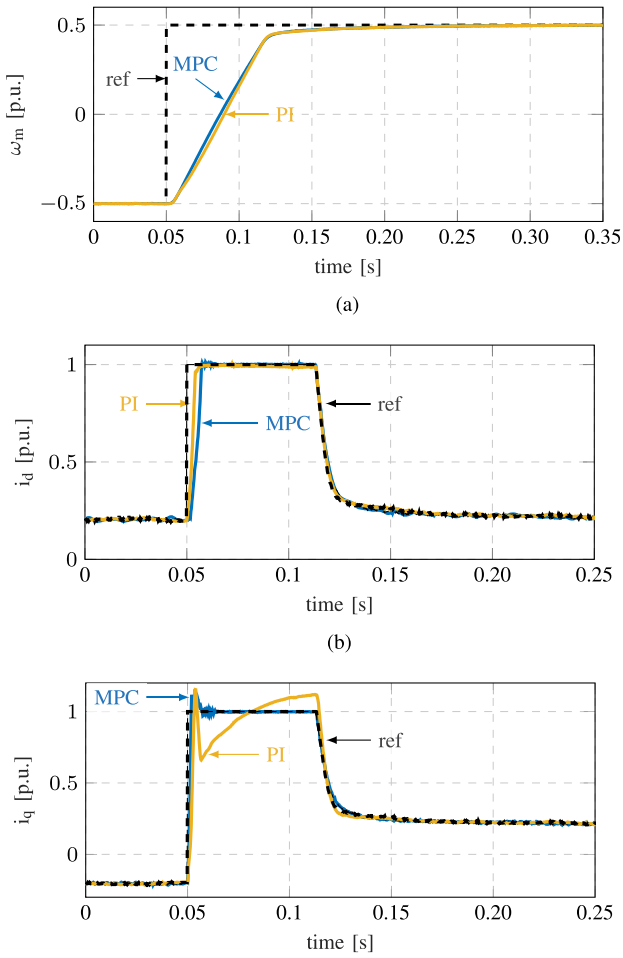

Fig. 10. Inverse speed test using MPC algorithm or PI-based current control for the SynR motor under test. (a) Speed response. (b) d-axis current response. (c) q-axis current response.

TABLE IV
MOTOR UNDER TEST NAMEPLATE PARAMETERS

Parameter	Symbol	Unit	SynR
DC voltage	u_{bus}	V	100
Resistance	R	Ω	4.76
d-axis inductance (unsat.)	L_d	mH	380
q-axis inductance (unsat.)	L_q	mH	85
Nominal current	I_n	A	4
Nominal speed	Ω_n	rpm	1500

the aVsIs solver. The model discussed in Section II-B was implemented in the MPC problem using the $\alpha\beta$ formulation of aVsIs discussed in Section III and the qpOASES solver for the sake of comparison. Two 50-Hz sinusoidal current references were applied, and the results are reported in Fig. 6. A step amplitude variation of the current reference was applied at 20 ms to force the voltage saturation. The voltage references obtained by the aVsIs and qpOASES solvers are reported in Fig. 6(b) and their difference in Fig. 6(c). The simulation results confirm that the aVsIs solver returns the same results of the qpOASES one.

The same test of Fig. 6 was carried out on an experimental test rig aiming at comparing the execution time of the proposed aVsIs with respect to the benchmark ones, i.e., qpOASES and qpSWIFT solvers. The system parameters are the same as those of the simulation test rig, i.e., the ones reported in Table III.

The current control measurements obtained by using the aVsIs solver are reported in Fig. 7(a). The current reference magnitude variation at 20 ms was forced to provoke the voltage saturation, as can be seen in Fig. 7(b).

The execution time of aVsIs, qpOASES, and qpSWIFT solvers is reported in Fig. 7(c). The aVsIs solver always required a smaller amount of time for completing the optimum voltage computation.

The aVsIs solver required a slight increment of execution time when voltage saturation occurred, which is due to the additional number of calculations listed in Table II and discussed in Section III. Actually, an execution time increment occurred for the qpOASES and qpSWIFT solvers as well.

B. Validation of the aVsIs Solver in dq

The dq solver proposed in Section IV was tested on a SynR motor electric drive application. The motor plate parameters are listed in Table IV.

Actually, the magnetic iron saturation was not considered, and the motor model for the MPC control structure can be found in [13]. It is worth recalling that the purpose of the article is to discuss the aVsIs solver for MPC problems; thus, the precise knowledge of the motor model is out of scope.

The speed reference was changed in a step-like fashion from 0% to 27% of the rated speed at 0.01 s, as reported in Fig. 8(b). The current references and measurements values are reported in Fig. 8(c). The space vector voltage trajectory is reported in the $\alpha\beta$ plane in Fig. 8(d). In particular, the transient behavior highlighted in the green-shaded area of Fig. 8(c) is also highlighted in green color in Fig. 8(d) to underline the hexagonal saturation of the voltage references. Finally, the comparison between the execution time obtained by using aVsIs, qpOASES, and qpSWIFT solvers is reported in Fig. 8(a). It can be noticed that the aVsIs solver is very efficient in terms of computational burden.

C. Comparison of Unconstrained and Constrained Solutions

Aiming at showing the advantages of using the constrained rather than the unconstrained $\mathbf{u}^{\text{unc}}$ solutions, the motor under test was dragged at $25\%\Omega_n$ by a prime mover. The bus voltage was set at 540 V. The current reference was changed on both axes to reach the 75% of the nominal current. The results using either constrained or unconstrained solutions, but saturated by the modulator, are reported in Fig. 9. The advantages in terms of current dynamics can be inferred from the results in Fig. 9.

D. Comparison With a Proportional–Integral (PI) Controller

The computational burden required by a PI linear regulator is linked to the complexity of its implementation. For instance, the adoption of antiwindup schemes, variable gains, and so forth increases the computational time to get the output. Experimental evidences returned that conventional PI-based current regulators required almost 1 μs using a dSPACE MicrolabBox, i.e., 0.8% of the control period. The proposed aVsIs-based MPC regulator required a maximum of 2 μs, i.e., 1.6% of the control period.

In order to compare the dynamic of the current tracking using either MPC-based or PI-based current regulators, a dedicated test was designed. The motor under test was speed controlled, without load, at half the rated value. The inverter bus voltage was 300 V to enhance the effect of the voltage saturation. The sign of the speed reference was suddenly inverted at time 0.05 s, as reported in Fig. 10(a). The speed controller forced an abrupt step-like change of the current references, as reported in Fig. 10(b) and (c). The MPC algorithm was based on (2) using constant parameters with the aid of a disturbance observer to achieve offset-free current tracking, e.g., [11]. The cost weight parameter was set at a constant value of 10^{-5}. For the sake of fairer comparison, the PI regulators were implemented using constant motor parameters for the design, e.g., those in Table IV. The axis decoupling was also implemented using constant parameters. On the one hand, the rise time of both controllers are similar. On the other hand, the current reference tracking is guaranteed by the MPC-based drive, whereas the PI-based one cannot efficiently reject the disturbance due to the speed variation.

VI. CONCLUSION

In this article, an analytical-solution-based solver for a wide class of indirect MPC algorithm with the hexagonal constraint for power electronic and electric drive application was proposed. The algorithm was presented in both the $\alpha\beta$ and dq reference frames to cover all the aforementioned applications. The proposed solver, aVsIs, requires a fixed number of operation in the worst-case scenario, which allows us to evaluate the implementation of MPC algorithms in every microcontroller. Both the simulation and experimental tests were performed highlighting the computational time required by the proposed solver compared with two general ones. Since the proposed solver returns an analytical solution of the problem, it can be

considered a benchmark for other solvers related to the same MPC control structure reported in Section II.

The MATLAB code of the proposed solver adopted in this article is available in Code Ocean. The code of the solver and its future developments are available at https://github.com/edlabVI/aVsIs.

REFERENCES

[1] P. Cortes, M. P. Kazmierkowski, R. M. Kennel, D. E. Quevedo, and J. Rodriguez, "Predictive control in power electronics and drives," *IEEE Trans. Ind. Electron.*, vol. 55, no. 12, pp. 4312–4324, Dec. 2008.

[2] J. Rodriguez et al., "Latest advances of model predictive control in electrical drives—Part I: Basic concepts and advanced strategies," *IEEE Trans. Power Electron.*, vol. 37, no. 4, pp. 3927–3942, Apr. 2022.

[3] J. Rodriguez et al., "Latest advances of model predictive control in electrical drives—Part II: Applications and benchmarking with classical control methods," *IEEE Trans. Power Electron.*, vol. 37, no. 5, pp. 5047–5061, May 2022.

[4] P. Karamanakos and T. Geyer, "Guidelines for the design of finite control set model predictive controllers," *IEEE Trans. Power Electron.*, vol. 35, no. 7, pp. 7434–7450, Jul. 2020.

[5] A. A. Ahmed, B. K. Koh, and Y. I. Lee, "A comparison of finite control set and continuous control set model predictive control schemes for speed control of induction motors," *IEEE Trans. Ind. Informat.*, vol. 14, no. 4, pp. 1334–1346, Apr. 2018.

[6] S. Vazquez, J. Rodriguez, M. Rivera, L. G. Franquelo, and M. Norambuena, "Model predictive control for power converters and drives: Advances and trends," *IEEE Trans. Ind. Electron.*, vol. 64, no. 2, pp. 935–947, Feb. 2017.

[7] P. Karamanakos, E. Liegmann, T. Geyer, and R. Kennel, "Model predictive control of power electronic systems: Methods, results, and challenges," *IEEE Open J. Ind. Appl.*, vol. 1, pp. 95–114, 2020.

[8] D. Kouzoupis, G. Frison, A. Zanelli, and M. Diehl, "Recent advances in quadratic programming algorithms for nonlinear model predictive control," *Vietnam J. Math.*, vol. 46, no. 4, pp. 863–882, 2018.

[9] R. Verschueren et al., "Acados: A modular open-source framework for fast embedded optimal control," *Math. Program. Comput.*, vol. 14, pp. 147–183, 2022.

[10] H. Ferreau, C. Kirches, A. Potschka, H. Bock, and M. Diehl, "qpOASES: A parametric active-set algorithm for quadratic programming," *Math. Program. Comput.*, vol. 6, no. 4, pp. 327–363, 2014.

[11] A. Favato, P. G. Carlet, F. Toso, R. Torchio, and S. Bolognani, "Integral model predictive current control for synchronous motor drives," *IEEE Trans. Power Electron.*, vol. 36, no. 11, pp. 13293–13303, Nov. 2021.

[12] A. Zanelli, J. Kullick, H. M. Eldeeb, G. Frison, C. M. Hackl, and M. Diehl, "Continuous control set nonlinear model predictive control of reluctance synchronous machines," *IEEE Trans. Control Syst. Technol.*, vol. 30, no. 1, pp. 130–141, Jan. 2022.

[13] S. Bolognani, S. Bolognani, L. Peretti, and M. Zigliotto, "Design and implementation of model predictive control for electrical motor drives," *IEEE Trans. Ind. Electron.*, vol. 56, no. 6, pp. 1925–1936, Jun. 2009.

[14] G. Cimini, D. Bernardini, S. Levijoki, and A. Bemporad, "Embedded model predictive control with certified real-time optimization for synchronous motors," *IEEE Trans. Control Syst. Technol.*, vol. 29, no. 2, pp. 893–900, Mar. 2021.

[15] M. Nauman and A. Hasan, "Efficient implicit model-predictive control of a three-phase inverter with an output LC filter," *IEEE Trans. Power Electron.*, vol. 31, no. 9, pp. 6075–6078, Sep. 2016.

[16] H. T. Nguyen, E.-K. Kim, I.-P. Kim, H. H. Choi, and J.-W. Jung, "Model predictive control with modulated optimal vector for a three-phase inverter with an LC filter," *IEEE Trans. Power Electron.*, vol. 33, no. 3, pp. 2690–2703, Mar. 2018.

[17] P. G. Carlet, A. Favato, S. Bolognani, and F. Dorfler, "Data-driven continuous-set predictive current control for synchronous motor drives," *IEEE Trans. Power Electron.*, vol. 37, no. 6, pp. 6637–6646, Jun. 2022.

[18] X. Liu et al., "Continuous control set predictive speed control of SPMSM drives with short prediction horizon," *IEEE Trans. Power Electron.*, vol. 37, no. 9, pp. 10166–10177, Sep. 2022.

[19] M. R. Arahal, C. Martín, A. Kowal, M. Castilla, and F. Barrero, "Cost function optimization for predictive control of a five-phase IM drive," *Optimal Control Appl. Methods*, vol. 41, no. 1, pp. 84–93, 2020.

[20] M. Bermúdez, F. Barrero, C. Martín, and M. Perales, "Performance analysis of direct torque controllers in five-phase electrical drives," *Appl. Sci.*, vol. 11, no. 24, 2021, Art. no. 11964.

[21] M. Bermúdez, C. Martín, I. González-Prieto, M. J. Durán, M. R. Arahal, and F. Barrero, "Predictive current control in electrical drives: An illustrated review with case examples using a five-phase induction motor drive with distributed windings," *IET Electr. Power Appl.*, vol. 14, no. 8, pp. 1291–1310, 2020.

[22] A. Favato et al., "Fast solver for implicit continuous set model predictive control of electric drives," *IEEE Access*, vol. 10, pp. 17430–17440, 2022.

[23] J. Yin, J. I. Leon, M. A. Perez, L. G. Franquelo, A. Marquez, and S. Vazquez, "Model predictive control of modular multilevel converters using quadratic programming," *IEEE Trans. Power Electron.*, vol. 36, no. 6, pp. 7012–7025, Jun. 2021.

[24] F. Toso, P. G. Carlet, A. Favato, and S. Bolognani, "On-line continuous control set MPC for PMSM drives current loops at high sampling rate using qpOASES," in *Proc. IEEE Energy Convers. Congr. Expo.*, 2019, pp. 6615–6620.

[25] J. Nocedal and S. J. Wright, *Sequential Quadratic Programming*. New York, NY, USA: Springer, 1999, pp. 526–573.

[26] F. Tinazzi, P. G. Carlet, S. Bolognani, and M. Zigliotto, "Motor parameter-free predictive current control of synchronous motors by recursive least-square self-commissioning model," *IEEE Trans. Ind. Electron.*, vol. 67, no. 11, pp. 9093–9100, Nov. 2020.

[27] A. Brosch, S. Hanke, O. Wallscheid, and J. Böcker, "Data-driven recursive least squares estimation for model predictive current control of permanent magnet synchronous motors," *IEEE Trans. Power Electron.*, vol. 36, no. 2, pp. 2179–2190, Feb. 2021.

[28] A. G. Pandala, Y. Ding, and H.-W. Park, "qpSWIFT: A real-time sparse quadratic program solver for robotic applications," *IEEE Robot. Autom. Lett.*, vol. 4, no. 4, pp. 3355–3362, Oct. 2019.

Ismaele Diego De Martin received the B.S. and M.S. degrees in mechatronics engineering in 2018 and 2021, respectively, from the University of Padova, Vicenza, Italy, where he is currently working toward the Ph.D. degree in mechatronics engineering with the Department of Management and Engineering.

His main research interests include predictive control techniques for ac motors.

Dario Pasqualotto (Member, IEEE) received the B.S. and M.S. (*cum laude*) degrees in mechatronics engineering in 2016 and 2018, respectively, from the University of Padova, Vicenza, Italy, where he is currently working toward the Ph.D. degree in mechatronics engineering with the Department of Management and Engineering.

His main research interests include modeling, predictive maintenance, and control techniques for ac motors.

Fabio Tinazzi (Member, IEEE) received the B.S., M.S., and Ph.D. degrees in mechatronic engineering from the University of Padova, Vicenza, Italy, in 2008, 2011, and 2015, respectively.

Since February 2017, he has been a Researcher with the Department of Management and Engineering, University of Padova. His main research interests include sensorless control, predictive control, and parameter estimation techniques for ac motors.

Open Access provided by 'Universita degli Studi di Padova' within the CRUI-CARE Agreement